Development of a new time domain-based algorithm for train detection and axle counting

Vehicle System Dynamics
Vol. 00, No. 00, March 2015, 1–25

RESEARCH ARTICLE

Development of a new time domain based algorithm for train detection and axle counting

B. Allotta[1], P. D'Adamio[1], E. Meli[1], L. Pugi[1]

[1] Department of Industrial Engineering, University of Florence,
via Santa Marta 3, 50139, Florence, Italy,
(*Received 00 Month 200x; final version received 00 Month 200x*)

1. Abstract

This paper presents an innovative train detection algorithm, able to perform the train localization and, at the same time, to estimate its speed, the crossing times on a fixed point of the track and the axle number. The proposed solution uses the same approach to evaluate all these quantities, starting from the knowledge of generic track inputs directly measured on the track (like, for example, the vertical forces on the sleepers, the rail deformation and the rail stress). More particularly, all the inputs are processed through cross-correlation operations to extract the required information in terms of speed, crossing time instants and axle counter. This approach has the advantage to be simple and less invasive than the standard ones (it requires less equipment) and represents a more reliable and robust solution against numerical noise because it exploits the whole shape of the input signal and not only the peak values.
A suitable and accurate multibody model of railway vehicle and flexible track has been also developed by the authors to test the algorithm when experimental data are not available and in general, under any operating conditions (fundamental to verify the algorithm accuracy and robustness). The railway vehicle chosen as benchmark is the Manchester Wagon, modelled in the Adams VI-Rail environment. The physical model of the flexible track has been implemented in the Matlab and Comsol Multiphysics environments. A simulation campaign has been performed to verify the performance and the robustness of the proposed algorithm, and the results are quite promising. The research has been carried out in cooperation with Ansaldo STS and ECM Spa.

Keywords: Train detection; Fiber Bragg grating sensor; Auto/Cross Correlation; Axle Counter

2. Introduction

With the increase of vehicle speed and traffic in the modern railways, a robust signalling system is fundamental to ensure the safety and reliable railway services [1]. In particular, the main safety properties of a reliable signalling system are the train detection, the railway traffic monitoring and the speed control on the train in the rear, to manage its movement according to the position of the train in front [2, 3]. Track circuits and axle

Corresponding author's e-mail: enrico.meli@unifi.it

ISSN: 0042-3114 print/ISSN 1744-5159 online

DOI: 10.1080/0042311YYxxxxxxxx
http://www.informaworld.com
https://doi.org/10.1080/00423114.2015.1084427

counters have been widely used to implement the train detection phase. Track circuits (see Fig. 1) refer to an electrical circuit with a power unit at one end of a track section and its functionality is based on the state of the receiver: when the signal arrives at the receiver, the complete circuit is close and becomes in the energized state [4, 5]. Otherwise, when a train is present, wheels shunt the track circuits and the receiver is de-energized.

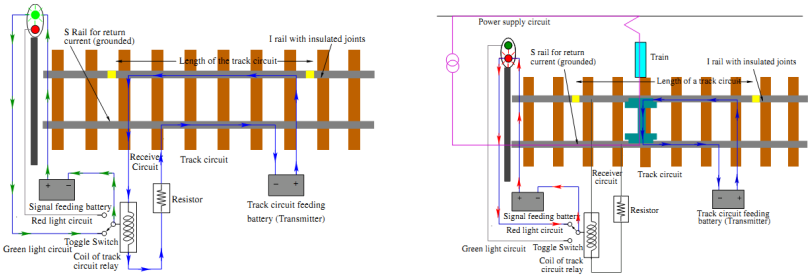

Figure 1.: Track circuit energized (left) and de-energized (right)

With the introduction of the electrification in railways, the rail is used both as track circuit and to carry the traction return current. To avoid interference (and to use less invasive solutions), the power source of the track circuit uses a different shape from that of the traction supply. However, an electromagnetic interference (EMI) is almost inevitable. The disadvantages of these solutions are their cost and the invasiveness for the railway track. For this reason and in order to have less invasive and expensive solutions, the axle counters have been widely used as alternative to the common track circuits. Axle counters do not rely on a physical closed electric circuit, but consist of a pair of electromagnetic coils mounted on both the sides of the rail head [6–8]. There are two axle counters, one transmitter and another one receiver and if the train is not present, a magnetic field is established between the coils (see Fig. 2). When a trail wheel is running on the rail and the coils, the magnetic field is perturbed and a change of the inducted voltage occurs. By reading the change of the inducted voltage, it is possible to detect the presence of the train [9].

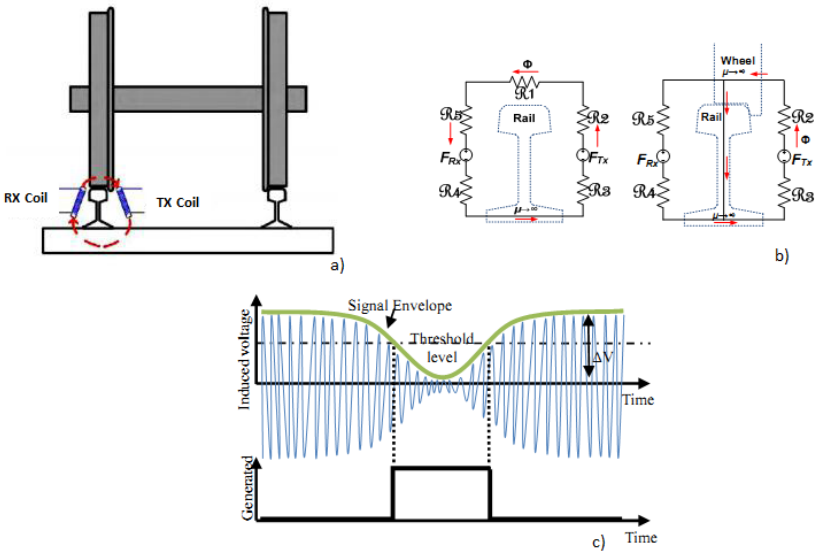

Figure 2.: Axle counter based on the electromagnetic technology: a) transmitter and receiver coil, b) corresponding electromagnetic circuit, c) inducted voltage on the receiver coil

Two sets of axle counters are installed at the two ends of a signalling block: the comparison of wheel passage count verifies if the train is in the block. However, as the operation depends on the delicate changes of magnetic field, EMI remains to be a genuine concern for the reliable operation of axle counters.
For this reason, many recent research works in literature propose a new simple sensor technology, the fiber Bragg grating sensor [10, 11], to be free from the EMI interference problem and to enhance the accuracy and reliability of the train detection of the signalling system [12, 13]. **Other works (see for example [14]) describe field tests concerning the application of fiber Bragg grating sensors to the detection of wheel flats in high-speed train wheels. Many other studies have studied the fiber Bragg sensor performances through experimental campaigns: C.L. Wei et.al [15] have developed a novel optical fiber sensor signalling system, providing an example of field setup, axle detection solution set and an installation in a trial system on a busy suburban railway line. Filograno et.al [16][17] showed many field tests concerning the application of fiber Bragg grating sensors for the monitoring of railway traffic, performed on the Spanish high-speed line Madrid-Barcellona.**
Using optical Bragg fiber technologies (see Fig. 3), any change of the shape of the profile of the wheel, also due for example to deterioration of the wheel/rail contact, is not a source of uncertainty. Besides, the FBG sensors are immune to electromagnetic interference (EMI): throughout the process, which begins with the detection of the signal up to its transmission to the interrogation system, there is no possibility of electromagnetic interference, due to degradation of integrity of the block axle counters.

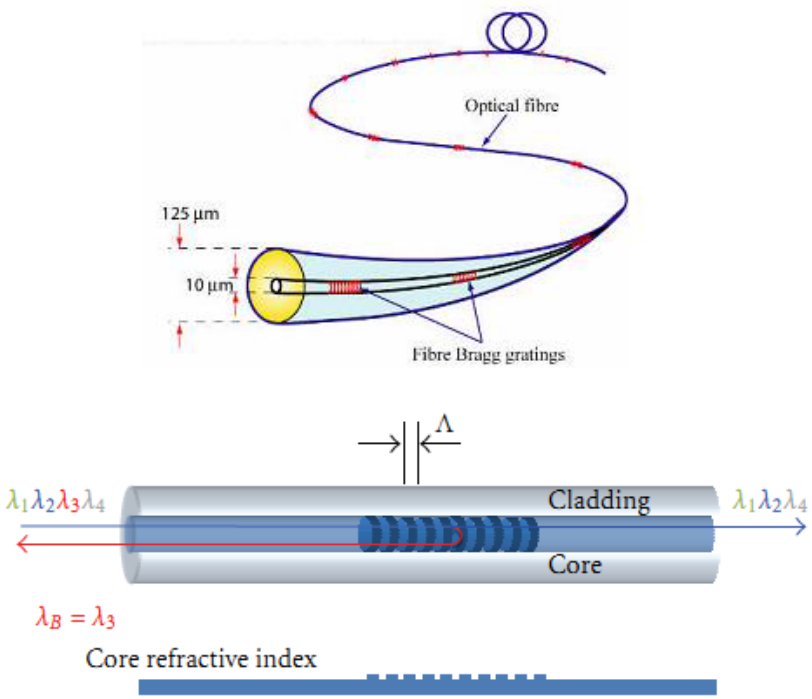

Figure 3.: Fiber Bragg technology: periodic modulation of the refractive index of the fiber core

Thanks to this innovative technology, the complexity of the measure system has moved from the sensor part to that of peak reading in the received signal. Chu-liang Wei et al. [15] have developed the X-Crossing and D-Crossing algorithms to compute the number of train axles crossing the measurement station: they have used a cut-off threshold followed by a derivative operation, to extract the useful peak corresponding to the crossing train axles from the received signals. T.K. Ho et al. [18] make the decomposition of the received

signals in different frequency band with the Wavelet Transform to study and define the spectral characteristics of the useful signal. Buggy et al. [19] make use of cut-off thresholds and derivative operation to implement the axle counter function. **As regards the speed detection, Kouroussis et al. [20][21] present a high precision train speed calculation technique based on ground vibration information for arbitrary train speeds.** These works are really important but are customized on a specific experimental input; consequently they do not offer a general approach to treat different experimental input signals, measurement chains and measurement layouts, and do not provide a satisfying robustness analysis against different signal-to-noise ratios on the input signal.
In this scenario, with the goal of obtaining a more general and reliable method, the studied work is collocated. The proposed train detection algorithm aims at providing the localization of the train, in terms of speed, crossing times on a fixed point of the track and axles number estimation. The formulation of the algorithm is quite general and it can be customized for several track measurement inputs (vertical loads on sleepers, stresses, strains, etc). Consequently it can be employed in different typologies of measurement stations and measurement chains: in the work case the chosen input is the vertical load on the sleeper [22].
Starting from the input signal, the estimation algorithm uses the cross-correlation to compute the crossing times of the train axles on the sleeper and consequently the vehicle speed; then, an operation of maximum peak detection, computed on the autocorrelations signal, followed by a time filtering based on a cut-off threshold, has been implemented to implement the axle counter function. All the post-processing operations are based only on auto and cross-correlation techniques and this represents a point of novelty for the proposed method, because it increases the simplicity and the reliability of the system. The algorithm is a low expensive and invasive method suitable for the Bragg fiber technology and is a robust solution against external noise and disturbances. The proposed approach turns out to be robust because, being based on correlation operations, it considers the global shape of the input signal, differently from other algorithms present in the literature that make use only of the local peaks of the measured signal.
A suitable multibody model of the railway vehicle (developed in Adams VI-Rail by the authors) and of the flexible track (developed in Matlab and Comsol) has been also developed to test the algorithm when experimental data are not available [23]. These two models interact online through a global contact model, developed by the authors in previous works [24, 25]. The considered railway vehicle is the Manchester Wagon [26]. The physical model of the system has been partially validated in the past by means of experimental data provided by Ansaldo STS [23]. These models are fundamental to test the algorithms in terms of accuracy and robustness under any operating conditions, also the most stressful ones.
A series of simulation campaigns has been made to test the algorithm performance and its robustness by varying the vehicle speed, the weights, the noise level on the input signal and the measurement layout and the results are quite promising. The research has been carried out in cooperation with Ansaldo STS and ECM S.p.a..

3. General architecture of the system

The architecture of the train detection system is composed of two parts: the physical model and the estimation algorithm. The input of the estimation model can be classified into two types: experimental data measured on the real railway track or, in absence of them, data provided by a physical model. The purpose of this arrangement consists in the possibility of testing the algorithm performance even when experimental data are not available, that is fundamental to test the algorithms under any operating conditions (not possible with experimental data).

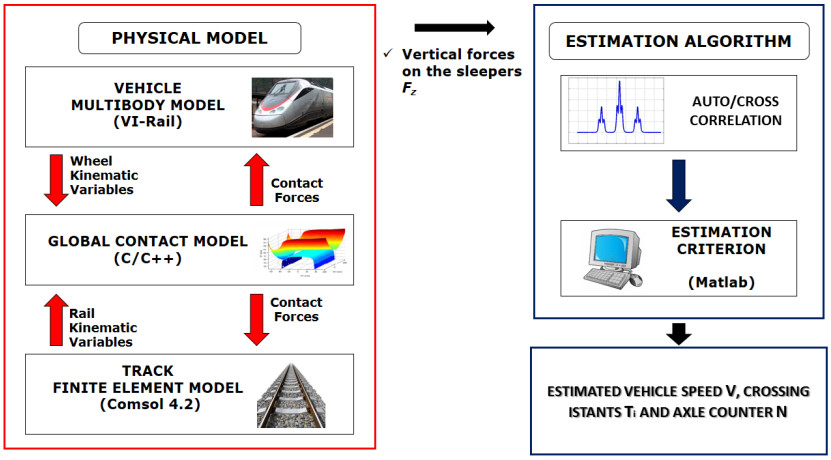

(a) General architecture of the system

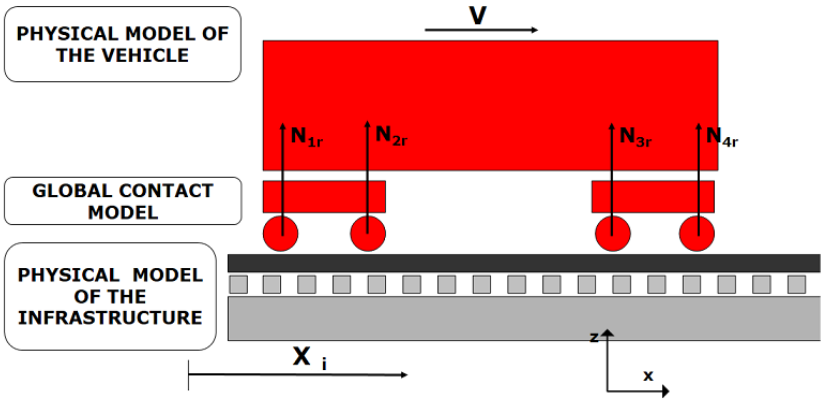

(b) Vehicle track and contact models: X_i indicates the i-th sleeper, as reported in Fig. 10

Figure 4.: General architecture of the system with a focus on the vehicle track and contact models

The physical model of the railway track consists of two sub-systems:

- 3D multibody model of the vehicle (in the studied case the Manchester Wagon [26]), implemented with VI-Rail software;
- 3D finite-element model (FEM) of the flexible railway track, developed in Comsol environment.

This two models interact online through a global wheel-rail contact model, developed by the authors in previous works [24][25]. The general architecture of the system and the physical model of the railway track are illustrated in Fig. 4a.
At each time integration step, the multibody model evaluates the kinematic variables (position, orientation and their derivatives) of each wheel; at the same time, the finite-element model (FEM) of the railway track evaluates the position, orientation and their derivatives for each node of the beam that represents the rail. Both the kinematic variables are then sent as inputs to the global contact model, that returns the global contact forces to be applied to the wheel and the rail.
Once the simulation is finished and the vertical forces on the sleepers $F^i_{z\,r/l}$, with i=1..N_{st} (N_{st} is the minimum i of measurement sleepers included in the measurement station) (indicating the vertical forces on the i-th sleeper measured at the right or left side of the train) are obtained, the estimation part begins. It is composed of two phases (both implemented

in Matlab): the first one computes the auto correlation of each input signal coming from the sleepers $F^i_{z\,r/l}$ and the cross-correlation among each pair of input signals $F^i_{z\,r/l}$, $F^j_{z\,r/l}$. The second phase, instead, aims at elaborating the signals previously obtained to determine the vehicle parameters as speed V, crossing times t_i on the i-th sleeper x_i and finally the number of train axles N. The signal processing operations used in the second phase will be described in detail in Chap. 4.

4. Train detection algorithm

The train detection algorithm aims at determining different train parameters like the crossing times of vehicle and wheelset on the sleepers, vehicle speed and axles number. The novelty of the proposed estimation method is that all these train quantities can be computed by means of only auto and cross-correlation operations. The used track inputs are the signals coming from the force sensors located on the left and right side on every sleeper $F^i_{z\,r}$, $F^i_{z\,l}$ (see Fig. 5 and Fig. 10), even if the algorithm can manage different signal input (i.e the vertical forces acting on the sleepers, the rail shear and bending, longitudinal strain and stress on rail). Fig. 5 illustrates the right and left vertical forces acting on the first sleeper (vehicle speed $V = 20\text{m}\,\text{s}^{-1}$ and car body mass $M = 40\text{t}$) of the measurement station: there are four peaks related to the four axles of the Manchester Wagon. **The left and right force signals are the signals coming from the sensors located at the left and right sides of the railway track (see Par. 5.4).**
In order to accurately reproduce the signal acquisition, different noise levels have been added to the input signal. For example, Fig. 5 represents two signals (with or without the added noise), in which a noise has been added on the input signal to obtain a signal input-to-noise ratio equal to 12 dB (vehicle speed $V = 20\text{m}\,\text{s}^{-1}$ and car body mass $M = 40\text{t}$). The considered signal is the mean between the left and right force input signals $\left(F^i_z = \frac{F^i_{z\,r}+F^i_{z\,l}}{2}\right)$, in order to reject possible disturbances due to the lateral motion of the vehicle. **The 3D multibody model of the vehicle and the flexible track provide realistic input signals, also including the possible effect due to the lateral vehicle dynamics and the train hunting. For these reason, the rejection of this effect (obtained through the mean between the left and right input signals) would not be possible by considering only one signal coming from the left or the right rail. In Fig. 5 the effect of the train hunting is negligible and, consequently, the difference between the right and left input signal is not relevant. However, if the train speed and the car-body mass increase, there are critical cases in which the hunting effect may become relevant and deeply affect the accuracy of the results.**

The first step consists, firstly, in performing the autocorrelation on each obtained signals F^i_z and then in the cross correlation between all the possible pairs of signals F^i_z and F^j_z. The generic expression of the cross-correlation between two signals (i,j) is:

$$\mathbf{R}_{ij}(m) = \sum_{n=0}^{N-m-1} F^i_{z_{(m+n)}} {F^j_{z_{(n)}}}^* \tag{1}$$

digitalized with N samples (m indicates the m-th sample of the correlation signals), where ${F^j_{z_{(n)}}}^*$ is the complex conjugate of the discretized signal j and $F^i_{z_{(m+n)}}$ indicates the discretized signal i, shifted of m samples. $R_{ii}(m)$ indicates the auto correlation signal. By means of the correlation operations, it is possible to evaluate the degree of true similarity between all the pairs of signals.

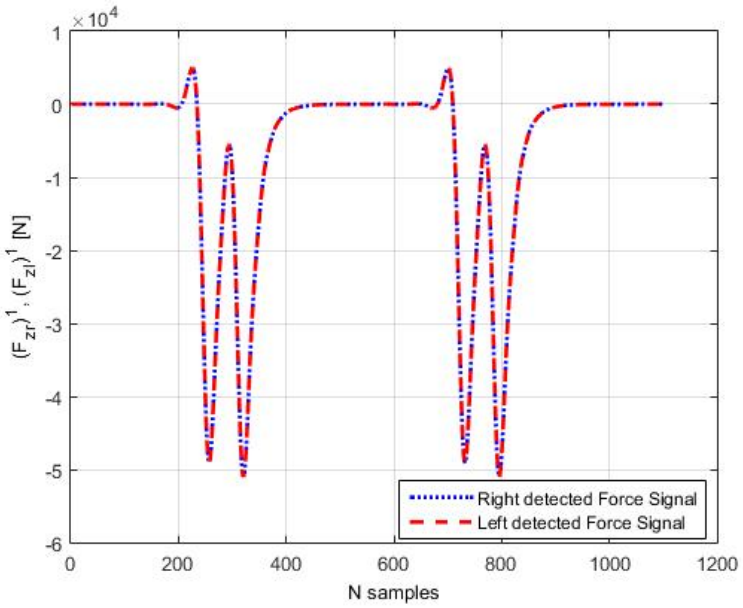

(a) Vertical forces F_{zr}^1, F_{zl}^1 acting on the right and left side of the first sleeper of the measurement station (performed at a vehicle speed V=20 m s^{-1}) and a car body mass M=40 t

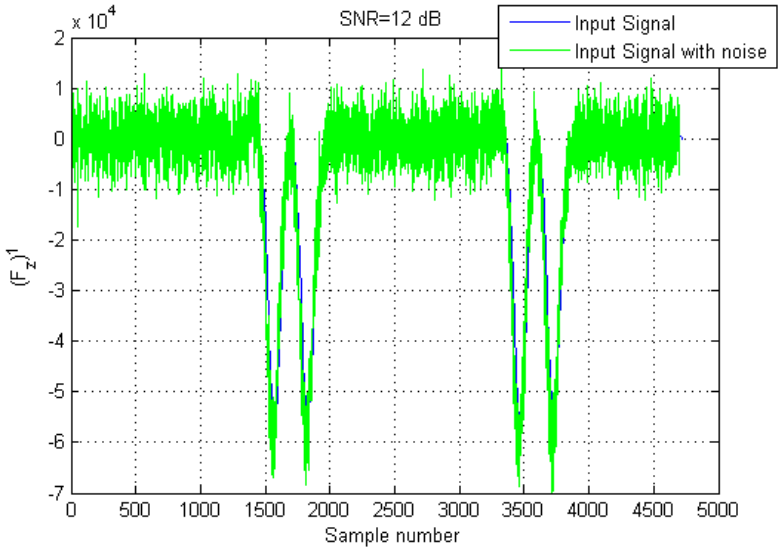

(b) Original input signal F_z^1 (red line) and input signal with added noise (green line): Signal-to Noise ratio (SNR)=12dB performed at a vehicle speed V=20 m s^{-1} and a car body mass M=40 t

Figure 5.: Input signal

In the second step, the attention is focused on the samples corresponding to the maximum value of the cross correlation signals: starting from the difference between the sample corresponding to the maximum value of the autocorrelation of the signal F_z^i and the one corresponding to its cross correlation with the F_z^j signal, it is possible to compute the time delay between the F_z^i, F_z^j signals just multiplying this difference by the sample time integration step Δt. Through this method, the time shifts between all the pairs of input signals can be easily determined. Once known the time delays, the vehicle speed can be computed just dividing the distance between the corresponding sleepers by the time shift previously found for the signals. An example with two sleepers located at X_i and X_j positions, spaced

of d_{ij} apart, is reported:

$$m_i = argmax\ \ R_{ii}(m) \qquad m_{ij} = argmax\ \ R_{ij}(m) \tag{2}$$

$$\Delta T_{ij} = \Delta t * |m_{ij} - m_i| = t_j - t_i \qquad d_{ij} = X_j - X_i \qquad V = \frac{d_{ij}}{\Delta T_{ij}} \tag{3}$$

where m_i and m_{ij} are the samples corresponding respectively to the maximum value of autocorrelation of i-th sleeper signal R_{ii} and cross correlation R_{ij} between the i-th and the j-th ones; Δt is the sample time and ΔT_{ij} is the time shift between the i-th and the j-th force signals (corresponding to the two sleepers); V represents the vehicle speed, computed dividing d_{ij} by the corresponding time delay ΔT_{ij}. Fig. 6a shows the case of time shift between the first and the tenth signals coming from the sleepers. Fig. 6 highlights also why the auto/cross correlation operations have been chosen to implement the estimation algorithm: the amplitude of the auto/cross correlation signal is bigger than that of the force signal coming directly from the sensor (see Fig. 5), and so it guarantees a major robustness against input noise and disturbances.
To compute the crossing times on sleepers it is sufficient to use the signal time shifts among the different sleepers, starting from the first one to the last one:

$$t_i = t_0 + \sum_{j=0}^{i-1} \Delta T_{j,j+1}. \tag{4}$$

The method used for the axle number detection is still based on the correlation theory: also in this case it has been decided to work with the correlation signals rather than the direct signals coming from the force sensors because the correlation operation increases the signals of several orders of magnitude when there is a good degree of true similarity and so it guarantees a better robustness against the input noise and disturbances. In addition, it has been observed that the peaks of true similarity, composing the correlation signal, are deeply related to the peaks of the original signal, representative of the passage of the axles on the sleepers. Fig. 6b illustrates the auto correlation signal when one, two or three of the axle peaks are present in the force signal instead of four.
The number of significant autocorrelation peaks is 9 if 4 axles are present, while decreases to 5 if 3 axles are present, decreases to 3 if 2 axles are present and finally decreases to 1 if 1 axle is present. Through this method, counting the autocorrelation peaks, it is possible to count the signal force peaks and hence the crossing train axles number.
Once the auto correlation signal is obtained, it has been limited inside a sample window, the size of which is determined to include only the significant samples. An algorithm to determine the signal local peaks is implemented, based on the signal $R_{i,i}$, on its derivative $R'_{i,i}$ and on suitable cut off thresholds to separate the signal peaks from the noise peaks [15].

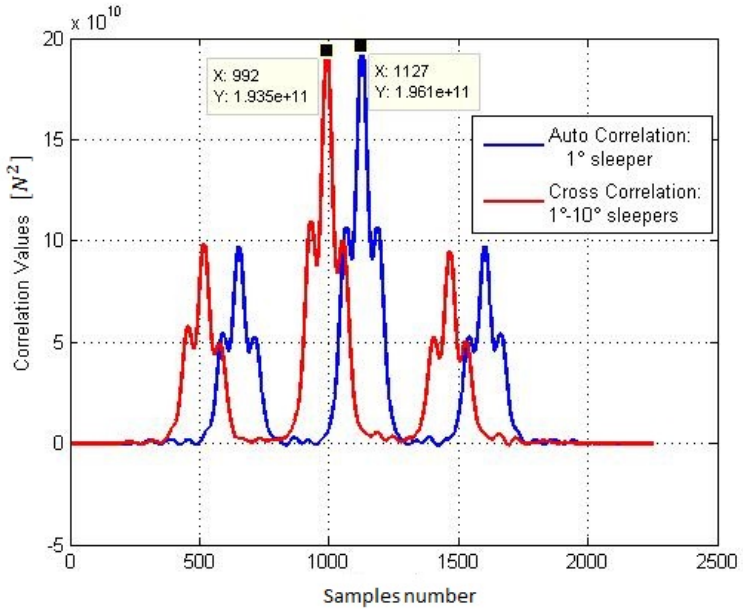

(a) Cross Correlation $R_{1,10}$ between the first sleeper signal F_z^1 and the tenth one F_z^{10} and the auto correlation $R_{1,1}$ of the signal F_z^1 (performed at a vehicle speed V=20 m s^{-1} and with a car body mass M=40 t)

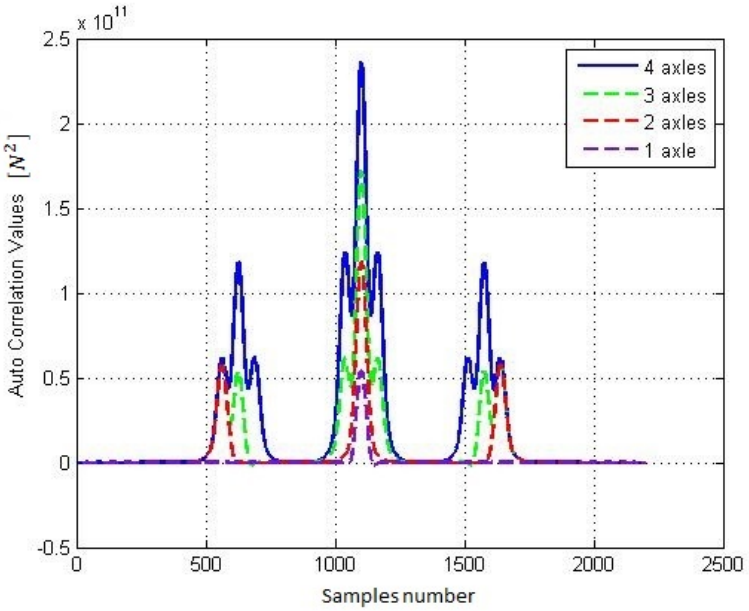

(b) Autocorrelation $R_{1,1}$ obtained with a different number of peaks present in F_z^1 (equal to 1,2,3,4 axles), performed at a vehicle speed V=20 m s^{-1} and with a car body mass M=40 t

Figure 6.: Cross Correlation and Auto Correlation techniques applied on input signals

5. Physical model of the railway track

The proposed train detection algorithm is independent from numerical models of railway tracks and vehicles. However, to generate suitable simulation campaigns to test and validate the algorithm under any operating conditions even when experimental data are not available, complete physical models involving all the system components [27][28][21] are required.

The physical model employed in this work consists of a 3D finite element model (FEM)

of the infrastructure (rail, sleepers and ballast), a 3D multibody model of the vehicle [25] and a contact model describing the interaction between the vehicle wheels and the rail. The vehicle model and the infrastructure model interact online during the simulations by means of the 3D global contact model, specifically developed to improve reliability and accuracy of the wheel-rail contact points detection.
The whole model can provide as outputs different track measurement signals like vertical loads on the sleepers, stresses and strains on the rail etc. In this work the vertical forces on the sleepers $F^i_{z\,r}$ and $F^i_{z\,l}$ are considered as inputs of the train detection algorithm (see Chapter. 4); (see Fig. 10).

5.1. *The infrastructure model*

Rail and infrastructures are modelled as 3D beams (see Fig. 7b), supported by an elastic discrete foundation representing sleepers and ballast (discretized through BEAM elements with two nodes for element and 6 DOFs for each node). The rails are connected through visco-elastic elements to n_{sl} 2D rigid bodies representing the sleepers, which are in turn supported by a visco-elastic foundation including the ballast properties (see Fig. 7b). The discretized equation of the rail is defined as:

$$M\ddot{\mathbf{q}}^{\mathbf{l/r}} + C\dot{\mathbf{q}}^{\mathbf{l/r}} + K\mathbf{q}^{l/r} = \mathbf{F}^{l/r} \tag{5}$$

in which M, C and K are the mass, damping and stiffness matrices of the track, $\mathbf{q}^{l/r}$ indicates the discretized track displacements and $\mathbf{F}^{\mathbf{l/r}}$ the external applied forces:

$$\mathbf{F}^{l/r} = \mathbf{F_{sl}}^{l/r} + \mathbf{F_c}^{l/r} \tag{6}$$

where $\mathbf{F_{sl}}^{l/r}$, $\mathbf{F_c}^{l/r}$ indicate the sleeper forces and the contact forces (provided by the vehicle and the global contact model). The variables of the generic node $\mathbf{q_i}^{l/r} \in R^6$ are the linear displacements $\mathbf{v} \in R^3$ and the rotational displacements $\theta \in R^3$:

$$\mathbf{q_i}^{l/r} = \begin{bmatrix} \mathbf{v_i}^{l/r} \\ \boldsymbol{\theta_i}^{l/r} \end{bmatrix} \tag{7}$$

where vector $\mathbf{v_i}^{l/r}$ includes longitudinal $u^{l/r}_{i_{rail}}$, lateral $v^{l/r}_{i_{rail}}$ and vertical $w^{l/r}_{i_{rail}}$ displacements expressed in the fixed reference system $O_{sys}x_{sys}y_{sys}z_{sys}$. The vector $\boldsymbol{\theta_i}^{l/r}$ indicates the rotational displacements $\phi^{l/r}_{i_{rail}}$, $\theta^{l/r}_{i_{rail}}$, and $\psi^{l/r}_{i_{rail}}$ expressed in the fixed reference system $O_{sys}x_{sys}y_{sys}z_{sys}$ (see Fig. 7a).
In this work the damping of the rail is modelled using the "proportional" or Rayleigh damping; the damping matrix $\mathbf{C}$ is evaluated as a linear combination of the inertia $\mathbf{M}$ and stiffness $\mathbf{K}$ matrices of the structure:

$$\mathbf{C} = \alpha_r\mathbf{M} + \beta_r\mathbf{K}. \tag{8}$$

The coefficients α_r and β_r are calibrated in order to fit the typical behaviour expected from experimental results and physical considerations available in literature [29–31].
In this work the UIC60 rail profile (with cant angle equal to 1/20) has been adopted. **The main physical characteristics of both rail beam model and sleepers-ballast system are referred to previous works [24][25]**.

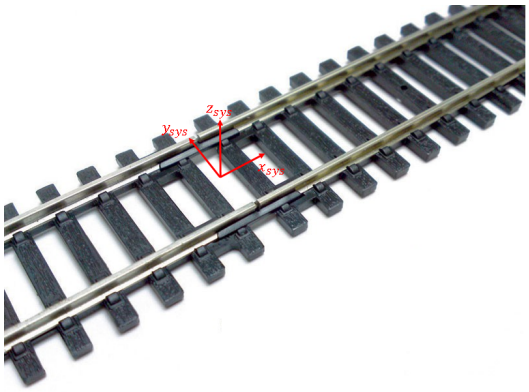

(a) Fixed reference system

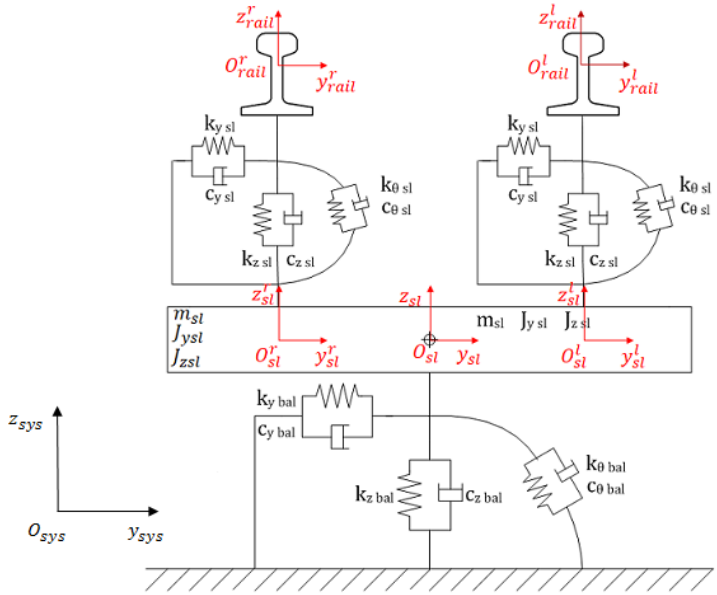

(b) Model of the interaction between rails, sleeper and ballast

Figure 7.: Reference system and infrastructure model

The length of the straight track studied in the model is $L = 72$m. The separation distance between two contiguos sleepers is equal to $l = 0.60$m. The sleepers are modelled as 2D rigid bodies connected to the rails by means of visco-elastic elements including lateral k_{ysl}, vertical k_{zsl} and rotational $k_{\vartheta sl}$ stiffness and lateral c_{ysl}, vertical c_{zsl} and rotational $c_{\vartheta sl}$ damping properties (see Fig. 7b). The longitudinal position $x_{sl\ p}$ of the $p-th$ 3DOF system modelling the sleepers-ballast ensemble can be expressed as follows:

$$x_{sl\ p} = L_I + (p-1)l, \qquad k = 1,2,...n_{sl} \tag{9}$$

where $x_{sl1} = L_I$, $x_{sl\ n_{sl}} = L_F$ (L_I and L_F are the beginning and the end of the track respectively), l is the distance between two contiguous sleepers and n_{sl} is the total number of sleepers.

The generic 2D sleeper is supported by a flexible foundation characterising the behaviour of the ballast through the lateral k_{ybal}, vertical k_{zbal} and rotational $k_{\vartheta ball}$ stiffness values and lateral c_{ybal}, vertical c_{zbal} and rotational $c_{\vartheta bal}$ damping values. m_{sl} and j_{sl} indicate the mass and inertia of sleepers.

The 3DOF body modelling the sleepers-ballast ensemble is described by the lateral y_{sl} and vertical z_{sl} translations and the rotation ϑ_{sl} around the $x_{sl} - axis$ of the sleeper reference

system expressed in the reference system $O_{sys}x_{sys}y_{sys}z_{sys}$ (see Fig. 7a).
Hence, the dynamic model of the sleeper can be expressed through the following equation:

$$M_{sl}\ddot{\mathbf{v}}_{sl}^{p} + \mathrm{K}_{sl}({\mathbf{v}_{sl}}^{p\,r} - {\mathbf{v}_{rail}}^{p\,r}) + \mathrm{C}_{sl}(\dot{\mathbf{v}}_{sl}^{p\,r} - \dot{\mathbf{v}}_{rail}^{p\,r}) + \mathrm{K}_{sl}({\mathbf{v}_{sl}}^{p\,l} - {\mathbf{v}_{rail}}^{p\,l}) + \\ + \mathrm{C}_{sl}(\dot{\mathbf{v}}_{sl}^{p\,l} - \dot{\mathbf{v}}_{rail}^{p\,l}) + \mathrm{K}_{bal}\mathbf{v}_{sl}^{p} + \mathrm{C}_{bal}\dot{\mathbf{v}}_{sl}^{p} = 0 \tag{10}$$

where subscript *sl* refers to the sleeper, subscript *bal* indicates the ballast properties, subscript *rail* is related to the rail and l/r refers to the left/right side of the rail. The vector ${\mathbf{v}_{sl}}^{p}$ includes lateral ${v_{sl}}^{p}$, vertical ${w_{sl}}^{p}$ and rotational ϕ^{p} displacement of the sleeper center of mass expressed in the fixed reference system $O_{sys}x_{sys}y_{sys}z_{sys}$ (see Fig. 7a); M_{sl} is the sleeper mass matrix while K_{sl} and C_{sl} are respectively the stiffness and damping matrices characterising the rail/sleeper visco-elastic connection. The K_{bal} and C_{bal} are respectively the stiffness and damping matrix of the ballast. The vectors ${\mathbf{v_{sl}}}^{p\,l}$,${\mathbf{v_{sl}}}^{p\,r}$ are defined as:

$${\mathbf{v_{sl}}}^{p\,r} = \begin{pmatrix} {v_{sl}}^{p\,r} \\ {w_{sl}}^{p\,r} \\ \phi^{p\,r} \end{pmatrix} = \begin{bmatrix} {v_{sl}}^{p} \\ {w_{sl}}^{p} - {\phi_{sl}}^{p}\frac{s}{2} \\ {\phi_{sl}}^{p} \end{bmatrix} \tag{11}$$

$${\mathbf{v_{sl}}}^{p\,l} = \begin{pmatrix} {v_{sl}}^{p\,l} \\ {w_{sl}}^{p\,l} \\ \phi^{p\,l} \end{pmatrix}, {\mathbf{v_{sl}}}^{p\,l} = \begin{bmatrix} {v_{sl}}^{p} \\ {w_{sl}}^{p} + {\phi_{sl}}^{p}\frac{s}{2} \\ {\phi_{sl}}^{p} \end{bmatrix} \tag{12}$$

where *s* indicates the railway gauge among the rails. The vectors ${\mathbf{v_{rail}}}^{p\,l}$,${\mathbf{v_{rail}}}^{p\,r}$ are defined as:

$${\mathbf{v_{rail}}}^{p\,r} = \begin{bmatrix} v_{rail}^{p\,r} \\ w_{rail}^{p\,r} \\ \phi_{rail}^{p\,r} \end{bmatrix}, \ {\mathbf{v_{rail}}}^{p\,l} = \begin{bmatrix} v_{rail}^{p\,l} \\ w_{rail}^{p\,l} \\ \phi_{rail}^{p\,l} \end{bmatrix}. \tag{13}$$

Therefore, each rail-sleeper interaction force is made up of the following components:

$$F_{y\,sl}^{l\,p}(t) = k_{y\,sl}(v_{sl}^{l\,p} - v_{rail}^{l\,p}) + c_{y\,sl}(\dot{v}_{sl}^{l\,p} - \dot{v}_{rail}^{l\,p}) \tag{14}$$

$$F_{y\,sl}^{r\,p}(t) = k_{y\,sl}(v_{sl}^{r\,p} - v_{rail}^{r\,p}) + c_{y\,sl}(\dot{v}_{sl}^{r\,p} - \dot{v}_{rail}^{r\,p}) \tag{15}$$

$$F_{z\,sl}^{l\,p}(t) = k_{z\,sl}(w_{sl}^{l\,p} - w_{rail}^{l\,p}) + c_{z\,sl}(\dot{w}_{sl}^{l\,p} - \dot{w}_{rail}^{l\,p}) \tag{16}$$

$$F_{z\,sl}^{r\,p}(t) = k_{z\,sl}(w_{sl}^{r\,p} - w_{rail}^{r\,p}) + c_{z\,sl}(\dot{w}_{sl}^{r\,p} - \dot{w}_{rail}^{r\,p}) \tag{17}$$

$$M_{x\,sl}^{l\,p}(t) = k_{\phi\,sl}(\phi_{sl}^{l\,p} - \phi_{rail}^{l\,p}) + c_{\phi\,sl}(\dot{\phi}_{sl}^{l\,p} - \dot{\phi}_{rail}^{l\,p}) \tag{18}$$

$$M_{x\,sl}^{r\,p}(t) = k_{\phi\,sl}(\phi_{sl}^{r\,p} - \phi_{rail}^{r\,p}) + c_{\phi\,sl}(\dot{\phi}_{sl}^{r\,p} - \dot{\phi}_{rail}^{r\,p}) \tag{19}$$

where $p = 1,2,..,n_{sl}$, ${v_{rail}}^{r/l\,p}$, ${w_{rail}}^{r/l\,p}$ and ${\phi_{rail}}^{r/l\,p}$ are the second, third and fourth element of the generic node variables ${\mathbf{q_i}}^{r/l\,p}$.

5.2. *The vehicle model*

The railway vehicle chosen for the dynamic simulations is the Manchester Wagon, the mechanical structure and the elastic and damping characteristics of which are easily available in literature [26].
The multibody 3D model of this vehicle has been widely studied and validated under different conditions. The model of the Manchester Wagon, implemented in the Adams VI-Rail environment, is schematically shown in Fig. 8a and it consists of seven rigid bodies: one car body, two bogies and four wheelsets.
The rigid bodies are connected by means of appropriate elastic and damping elements. More particularly, the vehicle is equipped with two suspension stages (see Fig. 8a, 8b and 8c) [26]. Both the suspension stages have been modelled through three-dimensional linear and nonlinear force elements like bushings, dampers and bumpstops. In this work the ORE S1002 wheel profile has been used.

5.3. *Global contact model*

The vehicle model and the infrastructure model interact online during the simulations by means of a 3D global contact model, developed by the authors in previous works, to improve the reliability and the accuracy of the contact points detection. In particular the used global contact model comprises both the contact points detection [24, 25] and the global contact forces evaluation, based on the theory of Hertz [27], Kalker [32, 33] and Polach [34]. The vehicle and infrastructure models calculate the wheel kinematics variables (related to each wheel) and the rail kinematics variables (related to each rail node). Starting from these quantities, the global contact model returns the global contact forces to be applied to the wheel and the rail. The global contact model is illustrated in Fig. 8d.

5.4. *Measurement Layout*

The train detection algorithm can manage different input signals measured on the track (vertical forces acting on the sleepers, rail deformations and stresses, etc.) and different measurement layouts characterized by various measure points (few if possible to reduce both the measure station dimensions and the economic costs) distributed along the railway track on both the track sides.
At this first step of the research activity, the vertical forces on the sleepers have been measured through force sensitive elements placed over the sleepers in the section corresponding to the rail baseplate/pads (see Fig. 9) [35].

The reference layout of the adopted measurement station consists of three measurement sleepers, each one equipped with two force sensors placed on both the rail sides (left/right). As represented in Fig. 10, the sensors are placed on three measurement sleepers (X_i indicates the position of the i-th sleeper).

A limited number of measurement sleepers (in this specific case 3) has to be chosen to not excessively increase the dimensions and the costs of the measurement station. On the other hand, the chosen measurement sleepers are consecutive to improve the robustness of the proposed approach. Considerations about the choice of measurement sleepers along the track can be found in [23][36].
In the near future, the proposed approach will be also tested using the rail deformations as track input. In this case, FBG sensors will be employed. The position of the sensors will be chosen starting from studies and experimental campaigns present in the literature. In [15] the optimal sensor position, corresponding to the maximum rail deformation is studied by means of the ANSYS Multiphysics software. Simu-

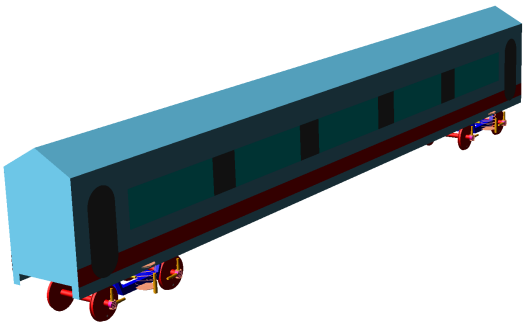

(a) Global view of the multibody model

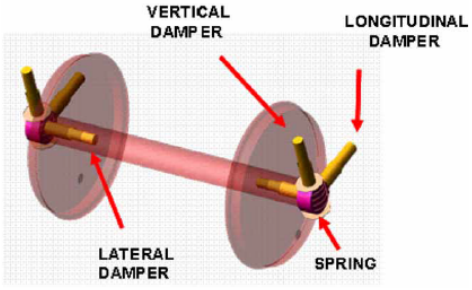

(b) Primary suspensions

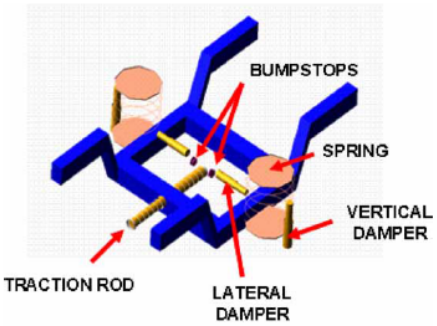

(c) Secondary suspensions

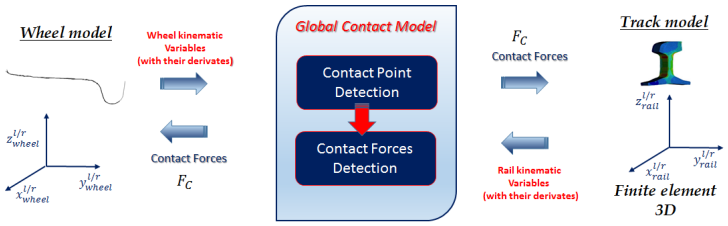

(d) Global contact model: interaction between the vehicle model and the finite element 3D model of the track

Figure 8.: Multibody model composition and global contact model

lation results highlight high deformation levels corresponding to the section on the rail head and rail foot. To validate the simulations, an experimental campaign is performed, considering FBG sensors placed on the rail head, web and foot both in vertical and longitudinal sections. Experimental results confirm the simulated ones, because the maximum deformation values are recorded by the longitudinal sensors placed on the rail head and rail foot: however, the first solution is not the best one due to railway safety requirements and so the optimal position is that of mounting sensors in the longitudinal section on the rail foot. If FBG sensor technology is employed, it is suggested to use another sensor, in addition to the previous one, placed

Figure 9.: Force sensitive elements placed over the sleepers

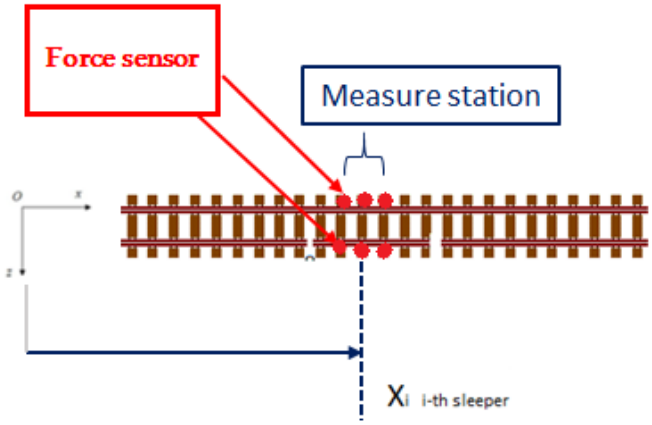

Figure 10.: Measurement Layout (position of the force sensors on the sleepers)

on the rail neutral line, in order to cut off the temperature effect [16].
During the next step of the research activity, in order to perform a preliminary validation of the proposed approach, sensing elements mounted on the rail foot and the rail neutral line will be tested. The sensors will be placed on the sections between two contiguous sleepers to further amplify the rail deformations. Once again, the measurement layout will consist of a limited number of consecutive measurement points to reduce dimensions and costs and to improve the system robustness.

6. Performance of the train detection algorithm in estimating the vehicle speed V and the crossing times t_i on the measurement sleepers

This chapter describes the performance of the train detection algorithm in estimating the speed and the crossing time instants on sleepers starting from the knowledge, among all the possible measurements inputs of the vertical loads on the sleepers. The estimation algorithm has been tested through a simulation campaign, in which the attention is focused on the estimation behaviour as a function of:

- vehicle speed (V);
- car body mass (M);

- input signal-to-noise ratio (SNR).

For the testing of the estimation algorithm performances, the reference measurement layout is the one reported in Fig. 10, composed of three force sensors located on the left and right side of three consecutive sleepers. In the following, as previously said, this layout will be modified so as to verify the robustness of the proposed estimation method. In Tab. 1a the considered ranges of the previous quantities are reported, where N_V, N_M, N_{snr} represent respectively the number of simulated values of V, M and signal to noise ratio SNR (the ratio between the power of the input signal and the one of noise input level).

Table 1.: Values of the simulation parameters (the speed V, the car body mass M and the signal-to -noise ratio SNR) in order to test the algorithm performance

(a) Variation ranges of V, M and SNR adopted for the simulation campaign in order to test the algorithm in estimating the crossing time instants t_i and the vehicle speed V

Parameter	**Min.**	**Max.**	$\mathbf{N_V/N_M/N_{snr}}$
Velocity ($\mathrm{m\,s^{-1}}$)	10	40	4
Car-body Mass (t)	10	50	5
Signal-to-noise ratio (dB)	5	12	4

(b) Variation ranges of V, M and SNR adopted for the simulation campaign aimed to test the algorithm as axles counter

Parameter	**Min.**	**Max.**	$\mathbf{N_V/N_M/N_{snr}}$
Velocity ($\mathrm{m\,s^{-1}}$)	10	40	4
Car-body Mass (t)	10	50	5
Signal-to-noise ratio (dB)	8	12	5

The global performance of the algorithm in terms of vehicle speed and the crossing times on the sleepers are reported and studied by considering the relative error $e^{sim}(V,M,SNR)$ on 100 different runs repeated according to the Monte Carlo approach for each value of M and V (the maximum error value is considered):

$$e_v^{sim} = \frac{|\widehat{V}^{sim} - V|}{V} \qquad e_{t_i}^{sim} = \frac{|\widehat{t_i}^{sim} - t_i|}{t_i} \tag{20}$$

where V and t_i represents the nominal values of the speed and crossing times respectively, and $\widehat{V}^{sim}$, $\widehat{t_i}^{sim}$ indicate the estimated ones. All the results are obtained with a time integration step equal to δT 0.001 s. Fig. 11a shows a comparison between the crossing times percentage errors, and their behaviour as a function of vehicle speed V and car body mass M; each graph is related to a different value of the signal to noise ratio SNR of the input signal (from 8 to 12 dB). In particular, for each SNR test case, the percentage errors on the second and third sleeper are reported (the first sleeper is assumed as reference and is coincident with a crossing time instant equal to zero).
The maximum resulting errors in the simulation campaigns are equal to 0.58 % and to 0.45 % for the second and third sleeper respectively, (related to a simulation performed considering the following values: V=30 $\mathrm{m\,s^{-1}}$, M=50 t and SNR = 5 dB).
The algorithm performances in estimating the crossing times on the sleepers are very important because the speed estimation uses the same time delays (between every pair of measurement sleepers) to perform the speed calculation: therefore an estimation error

on the time delays would deeply affect the estimation of the speed. The following figure (Fig. 11)b shows a comparison among the speed percentage errors and their behaviour as a function of vehicle speed V and car body mass M; each graph is related to a different value of the signal to noise ratio SNR of the input signal (from 5 to 12 dB).

The maximum error (equal to 0.54%) occurs in the case of the simulation performed considering the following values: V=30 m s^{-1}, M=30 t and SNR=5 dB.
The obtained results highlight the good performance of the algorithm against different values of input signal to noise ratio and consequently the capability of the algorithm to deal with measurement acquisition affected by a high noise level. Furthermore the increase of the vehicle speed and mass does not seem to influence the performance of the method. This is mainly due to the fact that, differently from other approaches present in the literature, the new algorithm exploits the global shape of the measurement signal, not only its local peaks. **Up to now, the performances of the algorithm have been tested and verified in the range 10-40 m/s; an important future development will consist in determining the highest measurement speed for the proposed approach.**

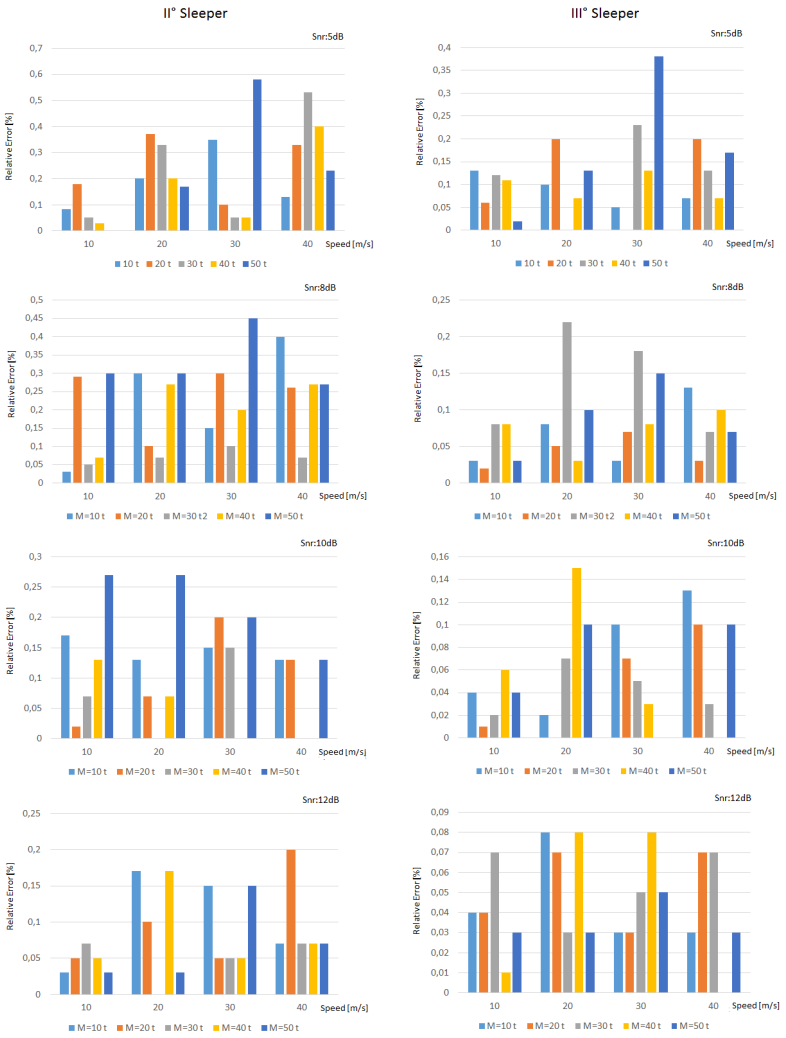

(a) Percentage relative error on the crossing times t_i on the second (on the left) and third (on the right) sleeper as a function of nominal speed V and car body mass M, for different values of SNR

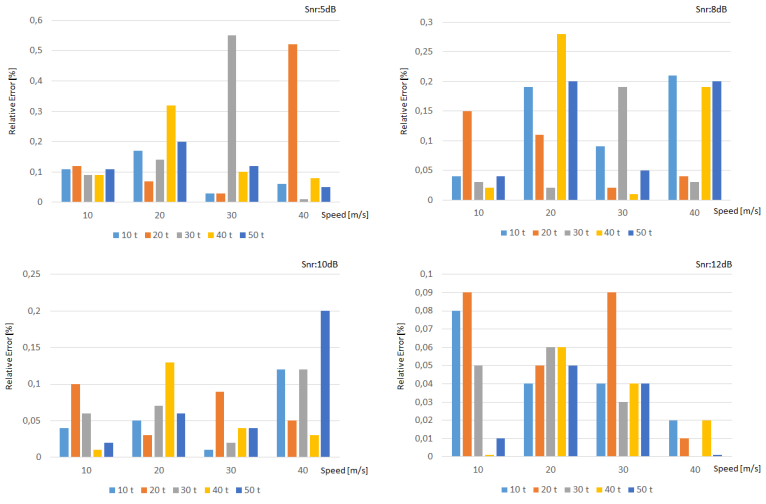

(b) Percentage relative error on the speed V as a function of nominal speed V and car body mass M, for different values of SNR

Figure 11.: Performance of the estimation algorithm in terms of percentage relative error on vehicle parameters

7. Performance of the train detection algorithm as axles counter

The simulation campaign to test the algorithm capability as axles counter has been performed with variable vehicle parameters and input noise as indicated in Tab. 1b.
The performance of the algorithm in estimating the train axles number has been evaluated considering the relative percentage error defined as follows:

$$e_N^{sim} = \frac{|\widehat{N}_{tot}^{sim} - N_{tot}|}{N_{tot}} \tag{21}$$

where N_{tot} represents the number of crossing vehicle axles and $\widehat{N}_{tot}^{sim}$ its estimated value. To test the axle counting performance, the results have been computed performing 100 runs of the algorithm, according to the Monte Carlo approach, for each value of vehicle speed V and car body mass M (the maximum error is considered). The used SNR values are those indicated in Tab. 2.

Table 2.: Error on estimating the axle number with variable speed V, car body mass M and SNR of the input signal

Speed [m s^{-1}]	Mass [t]	S/N=8db Err.[%]	S/N=9db Err.[%]	S/N=10db Err.[%]	S/N=11db Err.[%]	S/N=12db Err.[%]
	$M = 10t$	12	4	2	0	0
	$M = 20t$	17	3	1	0	0
10	$M = 30t$	18	5	1	1	0
	$M = 40t$	16	9	2	1	0
	$M = 50t$	15	10	3	1	1
	$M = 10t$	3	0	0	0	0
	$M = 20t$	5	0	0	0	0
20	$M = 30t$	6	3	1	0	0
	$M = 40t$	1	3	1	0	0
	$M = 50t$	8	2	1	0	0
	$M = 10t$	1	0	0	0	0
	$M = 20t$	1	0	0	0	0
30	$M = 30t$	3	2	0	0	0
	$M = 40t$	2	0	0	0	0
	$M = 50t$	6	2	2	0	0
	$M = 10t$	4	4	1	0	0
	$M = 20t$	12	3	3	2	1
40	$M = 30t$	10	5	3	0	0
	$M = 40t$	4	3	1	0	0
	$M = 50t$	3	3	0	0	0

Results show the good performance of the estimation algorithm as axles counter, especially with a SNR bigger than 10 dB (see Tab. 2)), in which the percentage errors are below than 3%. For each car body mass M and SNR of the input signal, the highest errors in the axle counting occur for the test case with speed V equal to 10 m s^{-1}: this further demonstrates the good performance of the algorithm, especially with high speed. Also in this case, an important role is played by the capability of the method to estimate the vehicle parameters starting from the global shape of the input signal, instead of only the local peaks.

8. Robustness of the train detection algorithm

In this section, the robustness of the algorithm is tested against different measurement layouts, that are modified by varying the number of the signal acquisition sleepers, the space among them and, consequently, the position of the measurement sleepers on the track. The results have always obtained for 100 runs of the algorithm according to the Monte Carlo approach and 16 measurement layouts have been tested. Tab. 3 indicates the characteristics of each measurement layout in terms of number of sleepers and space among the sleepers. The identification number of the sleepers along the track and of the considered layouts are also provided.

Table 3.: Characteristics of the measurement layouts in terms of number of measurement sleepers, space among them (equal to the number of sleepers included between two consecutive measurement sleepers), identification number of the sleepers and of the layouts

Number of sleepers	Spacing among sleepers	Sleeper ID	Layout ID
2	0	[64 65]	Layout 1
2	1	[64 66]	Layout 2
2	2	[64 67]	Layout 3
2	3	[63 67]	Layout 4
3	0	[64 65 66]	Layout 5
3	1	[64 66 68]	Layout 6
3	2	[62 65 68]	Layout 7
3	3	[60 64 68]	Layout 8
4	0	[53 64 65 66]	Layout 9
4	1	[60 62 64 66]	Layout 10
4	2	[58 61 64 67]	Layout 11
4	3	[56 60 64 68]	Layout 12
5	0	[63 64 65 66 67]	Layout 13
5	1	[60 62 64 66 68]	Layout 14
5	2	[58 61 64 67 70]	Layout 15
5	3	[56 60 64 68 72]	Layout 16

Tab. 4 illustrates the percentage errors in estimating the crossing times on sleepers t_i, while Tab. 5 indicates the percentage errors in estimating the vehicle speed V. All results are computed for different measurement layouts and vehicle car body masses M, with a fixed speed and a fixed signal to noise ratio (in the worst operating condition of V=40 $\mathrm{m\,s^{-1}}$ and SNR=5 dB). Results confirm the good capability of the algorithm in estimating the crossing times on sleepers and vehicle speed, against different measurement layout. All the estimation percentage error are below the 1 %.

Tab. 6 illustrates the estimation percentage errors on the axles number N_{tot} for different measurement layout, input signal to noise ratio SNR and vehicle car body mass M, with fixed vehicle speed (V=40 $\mathrm{m\,s^{-1}}$). Results show a better algorithm robustness with the increase of the sleepers number of the measurement layout.

The global performance in estimating the axles number are good with an input signal to noise ratio bigger than 10 dB, confirming the results obtained with the previous simulation campaign.

Table 4.: Percentage relative error on the crossing times on the sleepers t_i (Err.i indicates the error on the i-th sleeper of the layout) as a function of the measurement layout and car body mass M, for SNR=5 dB and vehicle speed V=40 m s^{-1}

Layout	Mass [t]	Err.1 [%]	Err.2 [%]	Err.3 [%]	Err.4 [%]	Err.5 [%]	Layout	Mass [t]	Err.1 [%]	Err.2 [%]	Err.3 [%]	Err.4 [%]	Err.5 [%]
	$M = 10t$	0	0.07	-	-	-		$M = 10t$	0	0.067	0.3	0.18	-
	$M = 20t$	0	0.20	-	-	-		$M = 20t$	0	0.53	0.17	0	-
Layout 1	$M = 30t$	0	0.87	-	-	-	Layout 9	$M = 30t$	0	0	0.03	0.18	-
	$M = 40t$	0	0.13	-	-	-		$M = 40t$	0	0.27	0.07	0.09	-
	$M = 50t$	0	0.67	-	-	-		$M = 50t$	0	0.35	0.05	0.08	-
	$M = 10t$	0	0.33	-	-	-		$M = 10t$	0	0.37	0.28	0.05	-
	$M = 20t$	0	0.03	-	-	-		$M = 20t$	0	0.26	0.08	0.04	-
Layout 2	$M = 30t$	0	0.1	-	-	-	Layout 10	$M = 30t$	0	0	0.05	0.078	-
	$M = 40t$	0	0.2	-	-	-		$M = 40t$	0	0	0.05	0.03	-
	$M = 50t$	0	0.17	-	-	-		$M = 50t$	0	0	0.04	0.05	-
	$M = 10t$	0	0.11	-	-	-		$M = 10t$	0	0.1	0	0.01	-
	$M = 20t$	0	0.15	-	-	-		$M = 20t$	0	0.15	0.17	0.04	-
Layout 3	$M = 30t$	0	0.07	-	-	-	Layout 11	$M = 30t$	0	0.24	0.18	0.05	-
	$M = 40t$	0	0.02	-	-	-		$M = 40t$	0	0.09	0.05	0.02	-
	$M = 50t$	0	0.04	-	-	-		$M = 50t$	0	0.09	0.01	0.02	-
	$M = 10t$	0	0.02	-	-	-		$M = 10t$	0	0.12	0	0.04	-
	$M = 20t$	0	0.07	-	-	-		$M = 20t$	0	0.07	0.07	0	-
Layout 4	$M = 30t$	0	0.02	-	-	-	Layout 12	$M = 30t$	0	0.08	0.13	0.04	-
	$M = 40t$	0	0.1	-	-	-		$M = 40t$	0	0.12	0.04	0.07	-
	$M = 50t$	0	0.04	-	-	-		$M = 50t$	0	0.04	0.02	0.03	-
	$M = 10t$	0	0.13	0.07	-	-		$M = 10t$	0	0.27	0.24	0.11	0.04
	$M = 20t$	0	0.33	0.2	-	-		$M = 20t$	0	0.13	0.17	0.13	0.07
Layout 5	$M = 30t$	0	0.53	0.13	-	-	Layout 13	$M = 30t$	0	0.27	0.04	0.02	0.07
	$M = 40t$	0	0.4	0.07	-	-		$M = 40t$	0	0	0.33	0.03	0.03
	$M = 50t$	0	0.23	0.174	-	-		$M = 50t$	0	0	0.27	0.16	0.07
	$M = 10t$	0	0.07	0.02	-	-		$M = 10t$	0	0.24	0.45	0.11	0.05
	$M = 20t$	0	0.07	0.21	-	-		$M = 20t$	0	0.12	0.18	0.15	0.07
Layout 6	$M = 30t$	0	0.14	0.02	-	-	Layout 14	$M = 30t$	0	0.38	0.05	0.02	0.07
	$M = 40t$	0	0.04	0.02	-	-		$M = 40t$	0	0.52	0.34	0.23	0.05
	$M = 50t$	0	0.21	0.07	-	-		$M = 50t$	0	0.43	0.28	0.12	0.04
	$M = 10t$	0	0	0.01	-	-		$M = 10t$	0	0.12	0.31	0.45	0.09
	$M = 20t$	0	0.12	0.01	-	-		$M = 20t$	0	0.32	0.21	0.07	0.04
Layout 7	$M = 30t$	0	0	0.07	-	-	Layout 15	$M = 30t$	0	0.24	0.04	0.15	0.03
	$M = 40t$	0	0	0.01	-	-		$M = 40t$	0	0	0.32	0.51	0.09
	$M = 50t$	0	0.14	0.04	-	-		$M = 50t$	0	0	0.04	0.21	0.10
	$M = 10t$	0	0.07	0.04	-	-		$M = 10t$	0	0.11	0.1	0.06	0.05
	$M = 20t$	0	0.04	0.03	-	-		$M = 20t$	0	0.02	0.03	0.07	0.04
Layout 8	$M = 30t$	0	0.27	0.12	-	-	Layout 16	$M = 30t$	0	0.18	0.04	0.09	0.05
	$M = 40t$	0	0.14	0.02	-	-		$M = 40t$	0	0.09	0.01	0.07	0.06
	$M = 50t$	0	0	0.02	-	-		$M = 50t$	0	0	0.27	0.16	0.07

9. Conclusion

In this paper the authors presented an innovative train detection algorithm with the aim of estimating the railway vehicle speed, its crossing time instants on the sleepers

Table 5.: Percentage relative error on the speed V as a function of the measurement layout and car body mass M, for SNR=5 dB and vehicle speed V=40 m s^{-1}

	$M = 10t$	0.68 %		$M = 10$t	0.18 %
	$M = 20t$	0.07 %		$M = 20t$	0.018 %
Layout 1	$M = 30t$	0.5 %	Layout 9	$M = 30t$	0.14 %
	$M = 40t$	0.42 %		$M = 40t$	0.26 %
	$M = 50t$	0.27 %		$M = 50t$	0.26 %
	$M = 10t$	0.04 %		$M = 10t$	0.19 %
	$M = 20t$	0.26 %		$M = 20t$	0.045 %
Layout 2	$M = 30t$	0.07 %	Layout 10	$M = 30t$	0.086 %
	$M = 40t$	0.14 %		$M = 40t$	0.17 %
	$M = 50t$	0.27 %		$M = 50t$	0.11 %
	$M = 10t$	0.07 %		$M = 10t$	0.13 %
	$M = 20t$	0.08 %		$M = 20t$	0.098 %
Layout 3	$M = 30t$	0.28 %	Layout 11	$M = 30t$	0.065 %
	$M = 40t$	0.07 %		$M = 40t$	0.086 %
	$M = 50t$	0.11 %		$M = 50t$	0.015 %
	$M = 10t$	0.007 %		$M = 10t$	0.049 %
	$M = 20t$	0.073 %		$M = 20t$	0.024 %
Layout 4	$M = 30t$	0.0067 %	Layout 12	$M = 30t$	0.043 %
	$M = 40t$	0.076 %		$M = 40t$	0.083 %
	$M = 50t$	0.008 %		$M = 50t$	0.012 %
	$M = 10t$	0.063 %		$M = 10t$	0.027 %
	$M = 20t$	0.52 %		$M = 20t$	0.21 %
Layout 5	$M = 30t$	0.013 %	Layout 13	$M = 30t$	0.072 %
	$M = 40t$	0.082 %		$M = 40t$	0.27 %
	$M = 50t$	0.052 %		$M = 50t$	0.12 %
	$M = 10t$	0.024 %		$M = 10t$	0.05 %
	$M = 20t$	0.011 %		$M = 20t$	0.03 %
Layout 6	$M = 30t$	0.05 %	Layout 14	$M = 30t$	0.02%
	$M = 40t$	0.11 %		$M = 40t$	0.08 %
	$M = 50t$	0.086 %		$M = 50t$	0.09 %
	$M = 10t$	0.12 %		$M = 10t$	0.03 %
	$M = 20t$	0.097 %		$M = 20t$	0.05 %
Layout 7	$M = 30t$	0.04 %	Layout 15	$M = 30t$	0.05 %
	$M = 40t$	0.03 %		$M = 40t$	0.05 %
	$M = 50t$	0.045 %		$M = 50t$	0.04 %
	$M = 10t$	0.1 %		$M = 10t$	0.003 %
	$M = 20t$	0.088 %		$M = 20t$	0.09 %
Layout 8	$M = 30t$	0.062 %	Layout 16	$M = 30t$	0.005 %
	$M = 40t$	0.042 %		$M = 40t$	0.01 %
	$M = 50t$	0.021 %		$M = 50t$	0.03 %

and finally its axles number. The algorithm is based on the measurement of the vertical forces on sleepers $F_{z\,r}^{i}$ and $F_{z\,l}{}^{i}$ performed through force sensitive elements placed over the sleepers in the section corresponding to the rail baseplate/pads. The novelty consists in using only correlation operations to estimate all the different parameters of the railway vehicle. A simulation campaign has been made to test the algorithm performance in estimating the vehicle parameters as a function of its speed V and

Table 6.: Error on the axles number N as a function of the measurement layout, the car body mass M and the signal to noise ratio SNR with a vehicle speed V=40 m s^{-1}

Layout	Mass [t]	SNR=8dB. Err.[%]	SNR=9dB Err.[%]	SNR=10dB Err.[%]	SNR=11dB Err.[%]	SNR=12dB [%]	Layout	Mass [t]	SNR=8dB Err.[%]	SNR= 9dB Err.[%]	SNR= 10dB Err.[%]	SNR= 11dB Err.[%]	SNR= 12dB [%]
	$M = 10t$	0	0	0	0	0		$M = 10t$	4	2	0	0	0
	$M = 20t$	2	1	1	1	1		$M = 20t$	5	0	0	0	0
Layout 1	$M = 30t$	3	2	1	1	0	Layout 9	$M = 30t$	2	2	1	1	0
	$M = 40t$	6	3	1	0	0		$M = 40t$	1	0	0	0	0
	$M = 50t$	9	5	2	2	2		$M = 50t$	5	3	2	0	0
	$M = 10t$	7	4	2	2	2		$M = 10t$	3	1	1	0	0
	$M = 20t$	9	3	0	0	0		$M = 20t$	2	1	0	0	0
Layout 2	$M = 30t$	5	2	0	0	0	Layout 10	$M = 30t$	4	0	0	0	0
	$M = 40t$	11	6	3	2	1		$M = 40t$	5	1	0	0	0
	$M = 50t$	7	3	0	0	0		$M = 50t$	0	0	0	0	0
	$M = 10t$	5	2	0	0	0		$M = 10t$	1	0	0	0	0
	$M = 20t$	5	2	0	0	0		$M = 20t$	3	0	0	0	0
Layout 3	$M = 30t$	5	4	3	2	0	Layout 11	$M = 30t$	5	2	0	0	0
	$M = 40t$	5	3	2	1	0		$M = 40t$	4	0	0	0	0
	$M = 50t$	16	8	4	3	0		$M = 50t$	4	3	1	0	0
	$M = 10t$	6	3	2	1	0		$M = 10t$	3	1	1	0	0
	$M = 20t$	6	3	1	0	0		$M = 20t$	2	1	1	0	0
Layout 4	$M = 30t$	4	3	2	1	0	Layout 12	$M = 30t$	3	0	0	0	0
	$M = 40t$	8	4	2	1	0		$M = 40t$	4	0	0	0	0
	$M = 50t$	11	5	3	1	0		$M = 50t$	7	2	0	0	0
	$M = 10t$	4	4	1	0	0		$M = 10t$	1	1	0	0	0
	$M = 20t$	12	3	3	2	1		$M = 20t$	3	2	0	0	0
Layout 5	$M = 30t$	10	5	3	0	0	Layout 13	$M = 30t$	2	2	0	0	0
	$M = 40t$	4	3	1	0	0		$M = 40t$	0	0	0	0	0
	$M = 50t$	3	3	0	0	0		$M = 50t$	0	0	0	0	0
	$M = 10t$	9	5	2	2	1		$M = 10t$	8	2	0	0	0
	$M = 20t$	3	1	1	0	0		$M = 20t$	2	1	1	1	0
Layout 6	$M = 30t$	5	4	4	1	0	Layout 14	$M = 30t$	1	1	0	0	0
	$M = 40t$	9	0	0	0	0		$M = 40t$	1	1	1	0	0
	$M = 50t$	1	3	0	0	0		$M = 50t$	1	1	0	0	0
	$M = 10t$	11	8	4	2	0		$M = 10t$	6	1	1	0	0
	$M = 20t$	7	6	3	0	0		$M = 20t$	2	1	0	0	0
Layout 7	$M = 30t$	10	4	2	2	1	Layout 15	$M = 30t$	3	2	1	0	0
	$M = 40t$	6	2	2	0	0		$M = 40t$	2	1	0	0	0
	$M = 50t$	2	0	0	0	0		$M = 50t$	2	1	0	0	0
	$M = 10t$	2	2	1	0	0		$M = 10t$	4	3	1	1	0
	$M = 20t$	9	6	5	0	0		$M = 20t$	1	4	0	0	0
Layout 8	$M = 30t$	4	3	0	0	0	Layout 16	$M = 30t$	4	2	1	0	0
	$M = 40t$	5	2	1	1	0		$M = 40t$	3	0	0	0	0
	$M = 50t$	5	0	0	0	0		$M = 50t$	4	0	0	0	0

car body mass M. In order to simulate different measurement operating conditions, the vehicle parameters have been estimated with a signal to noise ratio starting from 5dB up to 15 dB. Results highlight the good performance of the algorithm in performing the estimation of the crossing times on the sleeper and the vehicle speed in all the SNR range, showing a maximum relative estimation error less than 1 %. Good results have also been obtained testing the algorithm as axle counter through the Monte Carlo approach, with a maximum relative estimation error less than 2 % in all the SNR range. To test the algorithm robustness, a second simulation campaign has been performed, estimating the vehicle parameters (t_i, V and N) with different measurement layouts that differ from each other for the number of measurement sleepers and the distance among them. The obtained results confirm, also in this case, the performance of the algorithm and its robustness against different operative conditions and measurement layouts.

Concerning the future developments, the aim is to optimize the estimation algorithm as train axles counter, using lower SNR values and a variable composition of the

railway vehicle. Another future development will concern the testing of estimation algorithm with higher train speeds in order to find the maximum measurement speed for the proposed approach. From an experimental point of view, experimental tests are scheduled for the future by Ansaldo STS and ECM Spa. The experimental data will concern wagons travelling at high speeds and wagons characterized by different geometries.

References

[1] P.R. Goundan and A. Jhunjhunwala, *Axle counter based block signalling for safe and efficient train operations*, in *Vehicular Technology Conference*, Amsterdam, Holland, 19-22 Sep. 1999.
[2] J. Palmer, *The need for train detection*, in *Railway Signalling and Control Systems*, York, England, 5-9 June 2006.
[3] S.L. Ho, K.K. Lee, H.Y. Tam, W.H. Chung, S.Y. Liu, C.M. Yip, and T.K. Ho, *A Comprehensive Condition Monitoring of Modern Railway*, in *Railway Condition Monitoring*, Birmingham, England, 29-30 Nov. 2006.
[4] T. Akio, *Development of a trian detection system and a spread spectrum transmission system for track circuit*, in *Vehicular Technology Conference*, Phoenix, AZ, 4-7 May. 1997.
[5] S. Midya and R. Thottappillil, *An overview of electromagnetic compatibility challenges in Europoean Rail Traffic Management System*, Transportation Research PartC: Emerging Technologies 16 (2008), pp. 515–534.
[6] R. Bloomfield, *Fundamentals of European Rail Traffic Management System-ERMTS*, in *Proceedings of the 11th IET Professional Development Course on Railway Signalling and Control System*, York, England, 5-9 June 2006.
[7] J. Gadja, P. Piwowar, R. Sroka, M. Stencel, and T. Zeglen, *Application of inductive loops as wheel detectors*, Transportation Research PartC: Emerging Technologies 21 (2012), pp. 57–66.
[8] S. Zhang, W.K. Lee, and P.W.T. Pong, *Train Detection by Magnetic Field Measurement with Giant Magnetoresistive Sensors for High-Speed Railway*, Applied Mechanics and Materials 284-287 (2013), pp. 2102–2114.
[9] A. Zamani and A. Mirabadi, *Optimization of Sensor Orientation in Railway Wheel Detector, Using Kriging Method*, Journal of Electromagnetic Analysis and Applications 3 (2011), pp. 529–536.
[10] F. Mennella, A. Laudati, M. Esposito, A. Cusano, A. Cutolo, M. Giordano, S.Campopiano, and G.Breglio, *Railway monitoring and train tracking by fiber Bragg grating sensors*, in *Proc. SPIE 6619, Third European Workshop on Optical Fibre Sensors*, Napoli, Italy, 2 July 2007.
[11] L. Maurin, J. Boussoir, S. Rougeault, M. Bugaud, P. Ferdinand, A. Landrot, Y. Grunevald, and T. Chauvin, *FBG-based smart composite bogies for railway applications*, in *Optical Fiber Sensors Conference Technical Digest*, Portland,OR,USA, 10-10 May 2002.
[12] C. Wei, Q. Xin, W.H. Chung, S.Y. Liu, H.Y. Tam, and S.L. Ho, *Real-Time Train Wheel Condition Monitoring by Fiber Bragg Grating Sensors*, in *Proceedings of the 2010 Joint Rail Conference*, Urbana, IL,USA, 27-29 April 2010.
[13] W. Li, N. Jiang, J. Liu, and Y. Zhang, *Train axle counters by Bragg and chirped grating techniques*, in *19th International Conference on Optical Fibre Sensors*, Perth, Australia, 14 April 2008.
[14] M.L. Filograno, P. Corredera, M. Rodrguez-Plaza, A. Andrs-Alguacil, and M. Gonzlez-Herrez, *Wheel Flat Detection in High-Speed Railway Systems Using Fiber Bragg Gratings*, IEEE SENSORS JOURNAL 13 (2013), pp. 4808–4816.
[15] C.L. Wei, C.C. Lai, W.H. Chung, T.K. Ho, H.Y. Tam, S.L. Ho, A. McCusker, J. Kam, and K.Y. Lee, *A Fiber Bragg Grating Sensor System for Train Axle Counting*, Sensors Journal, IEEE 10 (2010), pp. 1905–1912.
[16] M.L. Filograno, A.R. Barrios, M.G. Herraez, P. Corredera, S. Lopez, M.R. Plaza, and A.A. Alguacil, *Real Time Monitoring of Railway Traffic Using Fiber Bragg Grating Sensors*, in *Joint Rail Conference*, Urbana, (IL)USA, 27-29 April 2010.
[17] M.L. Filogranov, P.C. Guillen, and A. Rodriguez-Barrios, *Real-time monitoring of railway traffic using fiber Bragg grating sensors*, IEEE SENSORS JOURNAL 12 (2012), pp. 85–92.
[18] T.K. Ho, S.Y. Liu, K.Y. Lee, Y.T. Ho, K.H. Ho, A. Maccusker, J. Kam, H.Y. Tam, and S.L. Ho, *An investigation of rail Condition monitoring by Fibre Bragg Grating sensors*, Transactions Hong Kong Institution of Engineers 16 (2009), pp. 9–15.
[19] S.J. Buggy, S.W. James, R. Carroll, J. Jaiswal, S. Staines, and R.P. Tatam, *Intelligent Infrastructure for Rail and Tramways Using Optical Fibre Sensors*, Journal of Sensors (2012).
[20] G. Kouroussis, D. Connolly, M. Forde, and O. Verlinden, *Train speed calculation using ground vibrations*, Journal of Rail and Rapid Transit DOI: 10.1177/0954409713515649 (2013).
[21] G. Kouroussis, O. Verlinden, and C. Conti, *Influence of some vehicle and track parameters on the environmental vibrations induced by railway traffic*, Veh.Syst.Dyn 50 (2012), pp. 619–639.
[22] V. Pavithradevi, D. Roopini, R.V.A. Aleem, and V.S. Shree, *Identification of the Presence of Train and its Formation*, in *Second National Conference on Trends in Automotive Parts Systems and Applications*, Tamilnadu, India, 21-22 March 2014.
[23] E. Meli and L. Pugi, *Preliminary development, simulation and validation of a weigh in motion system for railway vehicles*, Meccanica 48 (2013), pp. 2541–2565.
[24] E. Meli, S. Falomi, M. Malvezzi, and A. Rindi, *Determination of wheel - rail contact points with semianalytic methods*, Multibody System Dynamics 20 (2008), pp. 327–358.
[25] S. Falomi, M. Malvezzi, and E. Meli, *Multibody modeling of railway vehicles: innovative algorithms for the detection of wheel-rail contact points*, Wear 271 (2011), pp. 453–461.
[26] S. Iwnicki *The Manchester Benchmarks for Rail Vehicle Simulators*, Swets and Zeitlinger, Lisse, Netherland, 1999, 2008.
[27] W. Zhai and X. Sun, *A detailed Model for Investigating Vertical Interaction between Railway Vehicle and Track*, Veh.Syst.Dyn 23 (1994), pp. 603–615.
[28] C. Andersson and J. Oscarsson, *DYNAMIC TRAIN/TRACK INTERACTION INCLUDING STATE-DEPENDENT TRACK PROPERTIES AND FLEXIBLE VEHICLE COMPONENTS*, Veh.Syst.Dyn 33 (1999), pp. 47–58.
[29] S. Iwnicki *Handbook of Railway Vehicle Dynamics*, Taylor and Francis, 2006.
[30] T. Dahlberg, *Some railroad settlement models - a critical review*, Journal of Rail and Rapid Transit 215 (April 2001), pp. 289–300.
[31] J.A. Zakeri, H. Xia, and J.J. Fan, *Dynamic responses of train-track system to single rail irregularity*, Latin American Journal of Solids and Structures 6 (2009).
[32] J.J. Kalker *Three-dimensional Elastic Bodies in Rolling Contact*, Kluwer Academic Publishers, Dordrecht, Netherlands, 1990.
[33] J.J. Kalker, *A fast algorithm for the simplified theory of rolling contact*, Veh.Syst.Dyn 11 (1982), pp. 1–13.
[34] O. Polach, *A fast wheel-rail forces calculation computer code*, Veh.Syst.Dyn 33 (1999), pp. 728–739.
[35] *http://www.stockequipment.com*, Official site of Stock Equipment Company, 2012.
[36] M. Ignesti, A. Innocenti, L. Marini, E. Meli, L. Pugi, and A. Rindi, *Development of an Innovative Weigh In Motion System for Railways Vehicles*, in *Proceedings of the Multibody Dynamics Congress (ECCOMAS)*, Zagreb, Croatia, 2013.